# Simulation details

The computational model describes the dynamic mechanical interactions between short microtubules, long microtubules, and kinetochores in two spatial dimensions. All positions described below are 2-dimensional. The coordinate system is assumed to be in the spindle frame, meaning the first component is along the spindle axis and the second component orthogonal to this axis.

## Simulation overview

The following dynamic quantities are tracked in the simulations and updated at each time step.

1. The spatial positions of each kinetochore, $x_1, x_2$, labeled arbitrarily. This allows for the computation of IKD and cTilt,

$$\begin{aligned} \text{IKD} &= \| x_1 - x_2 \| \\ \text{cTilt} &= \arccos\big((x_1 - x_2) \cdot e_1\big) / \| x_1 - x_2 \|, \end{aligned}$$

   where $e_1 = [1,0]$, the unit vector corresponding to the spindle axis.

2. The spatial positions of $S$ minus-end tips of short microtubules emanating from each kinetochore, $y_j^i$ for $j = 1, \dots, S$ and $i = 1,2$.

3. The state of minus-end tips of $S$ short microtubules emanating from each kinetochore, $q_j^i$ for $j = 1, \dots, S$ and $i = 1,2$. The state is either $q = b$ for bound or $q = b$ for bound to a particular long microtubule.

The long microtubules are considered to be static and infinitely long in the simulation, each determined by a point on the line and the plus-end orientation $\phi$. Note that the orientation dictates the polarity of the microtubule. For example, $\phi = 0$ and $\phi = \pi$ are antiparallel, that is, geometrically parallel with opposite polarity.

The time step of simulation, $\Delta t$, is fixed. The initial conditions are taken to be $\mathrm{IKD} = L_{\mathrm{spring}}$ and $\mathrm{cTilt}$ uniformly random. All short microtubules are initially in the unbound state and placed at positions uniformly radial to each kinetochore at distance $L_{\mathrm{short}}$.

Each timestep of the simulation contains two steps:

4. Process binding and unbinding events by calculating position-dependent rates and then simulating whether an event occurs, updating the appropriate states if so.
5. Compute mechanical forces based on positions and use these to update positions

Due to the dependence between the reaction rates and positions, time steps are chosen to be small, and rates are assumed to be constant within each time step. We will describe each of these sub-steps in further detail.

## Binding and unbinding

At each timestep, the rate of each possible reaction is computed based on current positions and states. These reactions are modeled as a Poisson process, where the probability of reaction with rate $\omega$ occuring in a small timestep $[t, t + \Delta t]$ is $p_{\mathrm{react}} = \omega \cdot \Delta t$.

### Binding

Binding can occur when a short MT tip is unbound and near a long microtubule. The binding rate between short MT tip $j$ and long microtubule $k$ is

$$k_{\mathrm{on}}^{j \to k} = \begin{cases} \omega_{\mathrm{on}} & \| y_j - d_k \| \leq R \\ 0 & \text{otherwise,} \end{cases}$$

where $d_k$ is the smallest distance from $y_j$ to the line characterized by $d_k$'s position and direction. In practice, this is straightforward to compute by projection.

In words, binding occurs at constant when the short MT tip is within radius $R$ of a long microtubule. The result of the binding event is that the state $q_j \to b$ and the position is fixed to the closest point on the microtubule $y_j \to d_k$.

**Unbinding**

There are two types of unbinding considered in the model. One is the short MT unbinding at its minus-end from a long MT and the other is unbinding at its plus end from the kinetochore, both only occurring when the short MT is bound on the plus end.

**Type 1 unbinding (plus-end from KT)**. The connection between short MTs and kinetochores is assumed to be dynamic and able to be broken. The rate at which this connection breaks is modeled to depend on the angle between the kinetochore and the short MT, stemming from the assumption that the physical connection would become strained at large angles[S1,S2].

For short MT $j$ bound to kinetochore $i$, this angle is measured by

$$\gamma_j^i = \frac{\left(y_i^j - x_i\right) \cdot (x_i - x_{ii})}{\| \, y_i^j - x_i \, \| \| \, x_i - x_{ii} \, \|}.$$

Here $ii$ corresponds to the other kinetochore index. Then, the unbinding rate is a monotonically increasing function of $\gamma$,

$$k_{\text{break}} = \omega_b\left[\tanh\left(-\alpha\gamma_j^i\right) + 1\right].$$

In words, if $\gamma \approx 1$, the short MT emenates straight out of the kinetochore, assumed to be the most stable connection. As mechanics occur, $\gamma \approx 0$ means that the short MT is orthogonal to the kinetochore and this connection breaks with dramatically increased frequency. Short MTs that are connected toward the kinetochore detach effectively immediately, as this is physically unrealistic. The $\alpha$ parameter controls the sensitivity of this mechanism to the angle. When this occurs, $q_j \to u$ and $y_j$ is placed at a uniformly random location $L_{\text{short}}$ distance away from the

kinetochore. That is, a new connection forms immediately and total number of short MTs is conserved. This assumption is justified if the number of short MT connections at the kinetochore interface is limited by the number of linkers.

**Type 2 unbinding (minus-end from long MT)**. The other type of unbinding corresponds to the minus-end of short MT $j$ unbinding from a long microtubule. Although this connection is assumed to be by a molecular motor whose unbinding rate is known to be force-dependent, we assume that the motor force relaxes quickly relative to the rest of the system and this becomes effectively constant,

$$k_{\text{off}} = \omega_{\text{off}}.$$

When this occurs, $q_j^i \to u$ and the position is maintained $y_j^i \to y_j^i$, allowing for the possibility of rebinding quickly after.

## Forces

The force between kinetochores is modeled as a spring with some stiffness and rest length. The force on kinetochore $i$ is

$$F_{\text{spring}}^i = \begin{cases} -k_{\text{spring}}\left(\| x_i - x_{ii} \| - L_{\text{spring}}\right)\dfrac{x_i - x_{ii}}{\| x_i - x_{ii} \|} & \| x_i - x_{ii} \| > L_{\text{spring}} \\ 0 & \text{otherwise.} \end{cases}$$

Rigid short microtubules are modeled as stiff springs, with a nearly fixed length enforced by the spring stiffness.

$$F_{\text{short},j}^i = -k_{\text{short}}\left(\| y_j^i - x_i \| - L_{\text{short}}\right)\frac{y_j^i - x_i}{\| y_j^i - x_i \|}.$$

Effectively an angular spring, we assume there is a force causing short MTs to maintain emanating an angle straight out of kinetochores. Since the tip is modeled as a point, this is

modeled as a force pulling the tip to the position $L_{\text{short}}$ distance away from the kinetochore in the direction of the KT-KT vector. Therefore, the angular force is

$$F^i_{\text{ang},j} = -k_{\text{ang}}\left[y^i_j - \left(x_i + L_{\text{short}}\frac{x_i - x_{ii}}{\| x_i - x_{ii} \|}\right)\right].$$

While bound, the motors exert a constant force $F_m$ on the tip of short MT $j$ in the minus-end direction of the long microtubule described by the unit vector in the direction $-\phi$

$$F^i_{\text{mot},j} = F_m e_{-\phi}.$$

The evolution of the kinetochores due to the forces exerted on it is described by the stochastic differential equation (SDE)

$$\eta_k \dot{x}_i = F^i_{\text{spring}} - \sum_{j=1}^{S} F^i_{\text{short},j} + \xi_k \zeta_i(t),$$

where $\zeta_i$ is a white-noise process corresponding to random fluctuations with magnitude controlled by $\xi_k$ and $\eta_k$ is the effective drag coefficient.

The short microtubule tips follow a similar evolution,

$$\eta_s \dot{y}^j_i = F^i_{\text{short},j} + F^i_{\text{ang},j} + 1_{q^i_j = b} F^i_{\text{mot},j} + \xi_s \zeta_{j,i}(t).$$

where $1.$ is an indicator function causing the motor force to only be exerted while bound. The SDEs are updated at each time step using the Euler-Maruyama scheme.

## Long MT configurations

In the main text, four long MT configurations are mentioned and elaborated upon here. In all configurations, the number long MTs is chosen to be large enough that no simulation reaches a boundary in the timeframe of 100 seconds. That is, the pattern is effectively periodic in both dimensions.

**Antiparallel uniform**. In this configuration, all microtubules are equidistant, with distance $D_1$, in the 2nd dimension and are infinitely long in the first. The orientation alternates between $\phi = 0$ and $\phi = \pi$.

**Antiparallel bundled**. $B$ (an even number) of microtubules within a bundle are equidistant with distance $D_2$ apart from one another, again with alternating $\phi = 0, \pi$ orientation, so the number of each polarity is equal in each bundle. The bundles are placed so that the centers of each bundle at a distance $D_1$ apart.

**Angled**. Reference positions (intercepts) of each microtubule are placed at $(0, z)$ where each $z$ is $D_1$ distance apart. The orientations are then chosen to alternate between $\phi = \pi/4$ and $\phi = -pi/4$, resulting in a square lattice of microtubules.

**Biased bundled**. $B$ (an even number) of microtubules within a bundle are equidistant with distance $D_2$ apart from one another. For a bias $b$, each microtubule is individually assigned $\phi = 0$ with probability $b$ or $\phi = \pi$ with probability $1 - b$. For instance, the $3{:}\,1$ ratio corresponds to $b = 1/4$ (or $3/4$ by symmetry of the model).

## Parameters

Many of the parameters in the computational model have been measured experimentally, although some with reported values spanning several orders of magnitude. In these cases, we chose values roughly in the middle of the range of values. The parameters chosen for simulations can be found in the table below.

Parameters relating to molecular motors and mechanical properties of the kinetochores are thoroughly measured. Parameters that increase the motor attachment rate or force generation lead to faster biorientation. Parameters relating to short microtubules are relatively unknown. Rough estimates regarding number and geometry were made from previous studies, but

mechanical interactions are completely unknown. The plots shown below present parameter sweeps over the unknown short microtubule parameters. Although the biorientation times do depend on each of these parameters, these timings are robust to an order of magnitude when varying each of these parameters by several.

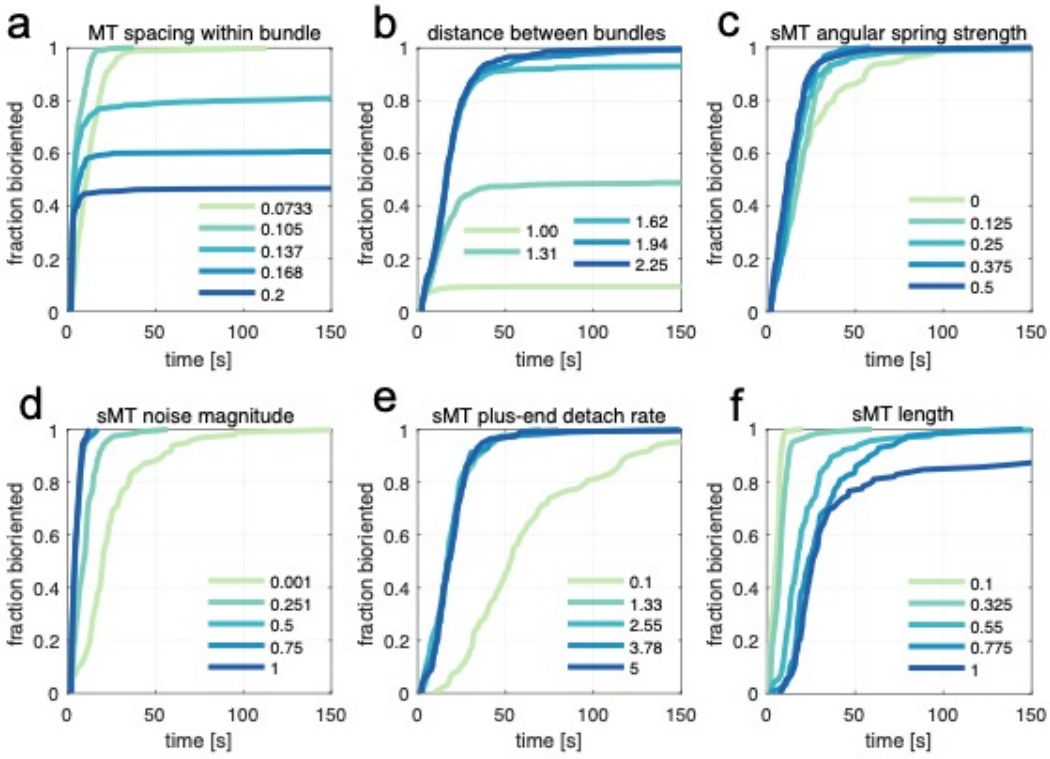


**Plots of additional parameter sweeps showing the dependence on various model parameters for biorientation times**. **a:** Biorientation becomes optimal values of intrabundle spacing, $D_2$, in the relevant on the order of 100 nanometers. **b:** Biorientation becomes favorable for more separated bundles, parameterized by the distance $D_1$. **c:** The angular spring stiffness $k_{\text{spring}}$ has little effect on the biorientation but does facilitate it slightly. **d:** More short microtubule fluctuations, parameterized by $\xi_s$ is favorable for biorientation. **e:** Short microtubules detaching at their plus end, the rate of which is parameterized by $\omega_b$ is necessary for

biorientation but does not improve the rate when made larger. **f:** Shorter short MTs, $L_{\mathrm{short}}$, are favorable for biorientation for the bundled configuration of long MTs only. In uniform (not shown), $L_{\mathrm{short}}$ on the order of hundreds of nanometers is optimal.

## Model parameters

| parameter | meaning | value(s) used in simulation | notes |
|---|---|---|---|
| $S$ | number of short MTs at each KT | varied, 0-40 | estimated from ref[S3] |
| $\omega_{\mathrm{on}}$ | binding rate | 10 $s^{-1}$ | notoriously difficult to measure, estimated magnitude from other motors[S4] |
| $R$ | binding radius | 75 nm | magnitude from dynein stalk length[S5] |
| $\omega_b$ | short MT plus-end breakage rate | 10 $s^{-1}$ | estimated to be on the timescale of motors unbinding |
| $\alpha$ | short MT plus-end breakage angular sensitivity | 100 | unknown, little effect on model behavior |
| $\omega_{\mathrm{off}}$ | short MT minus-end unbinding rate | 1 $s^{-1}$ | magnitude dynein unbinding rate under load[S6,S7] |
| $k_{\mathrm{spring}}$ | KT-KT spring stiffness | 60 pN/$\mu$m | magnitude from[S8-S10] |
| $L_{\mathrm{spring}}$ | KT-KT spring rest length | 0.65 $\mu$m | estimated from data |
| $k_{\mathrm{short}}$ | short MT stiffness | 500 pN/$\mu$m | approximately rigid[S11] |
| $L_{\mathrm{short}}$ | short MT length | 0.5 $\mu$m | estimated from ref[S3] |
| $k_{\mathrm{ang}}$ | short MT angular spring stiffness | 0.2 pN/$\mu$m | unknown |
| $F_m$ | short MT minus-end motor force | 3 pN | magnitude of force exerted by team of dynein |
| $\eta_k$ | kinetochore effective drag coefficient | 30 s·pN/$\mu$m | estimated from ref[S12-S14] |
| $\eta_s$ | short MT effective drag coefficient | 2 s·pN/$\mu$m | estimated as an order of magnitude smaller than KT drag coefficient |
| $\xi_k$ | kinetochore noise magnitude | 0.01 pN· $\mu$m | estimated, taken to be larger than thermal fluctuations alone, little effect on model behavior |
| $\xi_s$ | short MT tip noise magnitude | 0.1 pN· $\mu$m | unknown, estimated |
| $D_1$ | distance between long MT bundles | varied, ~2 $\mu$m | estimated[S11] |
| $D_2$ | distance between long MTs within bundles | varied, ~50 nm | estimated |
| $B$ | number of long MTs within bundle | varied, ~10 | estimated |
| $\Delta t$ | simulation time step | $10^{-3}$ | |

## Supplemental References


S1. Khataee, H., and Howard, J. (2019). Force Generated by Two Kinesin Motors Depends on the Load Direction and Intermolecular Coupling. Phys Rev Lett *122*, 188101. 10.1103/PhysRevLett.122.188101.

S2. Pyrpassopoulos, S., Shuman, H., and Ostap, E.M. (2020). Modulation of Kinesin's Load-Bearing Capacity by Force Geometry and the Microtubule Track. Biophys J *118*, 243-253. 10.1016/j.bpj.2019.10.045.

S3. Sikirzhytski, V., Renda, F., Tikhonenko, I., Magidson, V., McEwen, B.F., and Khodjakov, A. (2018). Microtubules assemble near most kinetochores during early prometaphase in human cells. J Cell Biol *217*, 2647-2659. 10.1083/jcb.201710094.

S4. Leduc, C., Campas, O., Zeldovich, K.B., Roux, A., Jolimaitre, P., Bourel-Bonnet, L., Goud, B., Joanny, J.F., Bassereau, P., and Prost, J. (2004). Cooperative extraction of membrane nanotubes by molecular motors. Proc Natl Acad Sci U S A *101*, 17096-17101. 10.1073/pnas.0406598101.

S5. Can, S., Lacey, S., Gur, M., Carter, A.P., and Yildiz, A. (2019). Directionality of dynein is controlled by the angle and length of its stalk. Nature *566*, 407-410. 10.1038/s41586-019-0914-z.

S6. Kunwar, A., Tripathy, S.K., Xu, J., Mattson, M.K., Anand, P., Sigua, R., Vershinin, M., McKenney, R.J., Yu, C.C., Mogilner, A., and Gross, S.P. (2011). Mechanical stochastic tug-of-war models cannot explain bidirectional lipid-droplet transport. Proc Natl Acad Sci U S A *108*, 18960-18965. 10.1073/pnas.1107841108.

S7. Tan, R., Foster, P.J., Needleman, D.J., and McKenney, R.J. (2018). Cooperative Accumulation of Dynein-Dynactin at Microtubule Minus-Ends Drives Microtubule Network Reorganization. Dev Cell *44*, 233-247 e234. 10.1016/j.devcel.2017.12.023.

S8. Banigan, E.J., Chiou, K.K., Ballister, E.R., Mayo, A.M., Lampson, M.A., and Liu, A.J. (2015). Minimal model for collective kinetochore-microtubule dynamics. Proc Natl Acad Sci U S A *112*, 12699-12704. 10.1073/pnas.1513512112.

S9. Sarangapani, K.K., Akiyoshi, B., Duggan, N.M., Biggins, S., and Asbury, C.L. (2013). Phosphoregulation promotes release of kinetochores from dynamic microtubules via multiple mechanisms. Proc Natl Acad Sci U S A *110*, 7282-7287. 10.1073/pnas.1220700110.

S10. Stephens, A.D., Haase, J., Vicci, L., Taylor, R.M., 2nd, and Bloom, K. (2011). Cohesin, condensin, and the intramolecular centromere loop together generate the mitotic chromatin spring. The Journal of Cell Biology *193*, 1167-1180. 10.1083/jcb.201103138.

S11. Letort, G., Nedelec, F., Blanchoin, L., and Thery, M. (2016). Centrosome centering and decentering by microtubule network rearrangement. Mol Biol Cell *27*, 2833-2843. 10.1091/mbc.E16-06-0395.

S12. Marshall, W.F., Marko, J.F., Agard, D.A., and Sedat, J.W. (2001). Chromosome elasticity and mitotic polar ejection force measured in living Drosophila embryos by four-dimensional microscopy-based motion analysis. Curr Biol *11*, 569-578.

S13. Nicklas, R.B. (1965). Chromosome Velocity during Mitosis as a Function of Chromosome Size and Position. J Cell Biol *25*, SUPPL:119-135. 10.1083/jcb.25.1.119.

S14. Nicklas, R.B. (1988). The forces that move chromosomes in mitosis. Annual Review of Biophysics & Biophysical Chemistry *17*, 431-449.